Hydrological Sciences Journal

ISSN: 0262-6667 (Print) 2150-3435 (Online) Journal homepage: http://www.tandfonline.com/loi/thsj20

Spatial patterns of frequent floods in Switzerland

Klaus Schneeberger, Ole Rössler & Rolf Weingartner

To cite this article: Klaus Schneeberger, Ole Rössler & Rolf Weingartner (2018): Spatial patterns of frequent floods in Switzerland, Hydrological Sciences Journal

To link to this article: https://doi.org/10.1080/02626667.2018.1450505

Accepted author version posted online: 29 Mar 2018.

Spatial patterns of frequent floods in Switzerland

Klaus Schneeberger[a,b,c], Ole Rössler[b], Rolf Weingartner[b,c]

[a]*alpS - Centre for Climate Change Adaptation, Grabenweg 68, AT-6020 Innsbruck, Austria*

[b]*Institute of Geography, Hydrology Group, University of Bern, Hallerstrasse 12, CH-3012 Bern, Switzerland*

[c]*Oeschger Centre for Climate Change Research, Bern, Switzerland*

Contact: klaus.schneeberger@gmx.net

Abstract This study investigates the spatial dependence of high and extreme streamflows in Switzerland across different scales. First, using 56 runoff time series from Swiss rivers, we determined the average length of high-streamflow events for different levels of extremeness. Second, a dependence measure that expressed the probability that streamflow peaks would meet or exceed streamflow peaks at a conditioning site was used to describe and map the spatial extent of joint streamflow-peak occurrences across Switzerland. Third, we analysed the spatial patterns of jointly occurring high streamflows using cluster analysis to identify groups that react similarly in terms of flood frequency at different sites. The results indicate that, on a coarse scale, high and extreme streamflows are asymptotically independent in the main Swiss basins. Additionally, meso-scale tributaries in the main basins show distinct flood regions across river systems.

Keywords frequent floods; temporal dependence; spatial dependence; cluster analysis; Switzerland

Introduction

During the past decade, Europe has experienced frequent flood events that caused multiple fatalities and direct economic damage (Kundzewicz 2015). An increase of flood damages is often attributed to climate change. However, the picture is more

complex. Flood related economic damages are observed to have increased due to societal factors (Barredo 2009), i.e. a significant increase of the values at risk since the 1950s (Hilker *et al.* 2009). Moreover, a clear European-wide increasing trend of flood frequencies is not detectable (Hall *et al.* 2014; Madsen *et al.* 2014). However, for Switzerland, Castellarin and Pistocchi (2012) found an increase in flood peaks in alpine areas of 20% irrespective of return periods that correlates with an increase of mean temperature and hence likely climate change. A challenge for such conclusions is the frequently found temporal clustering of flood events (Schmocker-Fackel and Naef 2010; Merz *et al.* 2016) that prevent a straightforward interpretation. Regardless of whether flood frequencies already changed with climate change, Köplin *et al.* (2014) projected an increase in flood frequencies for northern Switzerland. Not least because of this future challenge, there is a great need to mitigate floods and their related negative impacts. Therefore, coordinated risk-oriented flood management is considered as a major mitigation measure.

One essential element of successful flood management is the spatial delineation of expected flood depth and velocity given a certain flood magnitude (Excimap 2007). One major drawback of these inundation maps is that they cannot depict the interregional heterogeneity of individual flood events. More precisely, a 100-year flood will not occur everywhere at the same time; rather, it forms an event-specific extent that may spread across different basins and stretch over different orders of magnitudes.

Historically, information on the spatial characteristics of a flood and the accompanying consequences (e.g. economic damage) were gathered widely from *a posteriori* analysis of the flood event and from the hydro-meteorological conditions that led to the catastrophe (e.g. Becker and Grünewald 2003, Bezzola and Hegg C. 2007, Blöschl *et al.* 2013, Schröter *et al.* 2015, Thieken *et al.* 2016). *A priori* analyses of

potential flood areas that are likely to be affected by flood events are often missing. Recent studies have shown the importance of considering both spatially heterogeneous and consistent flood patterns (e.g. Moel *et al.* 2015, Falter *et al.* 2015, Falter *et al.* 2016, Schneeberger *et al.* 2017). This information is of great value and can be used to correctly estimate the maximal affected area and the potential direct economic damage for an individual event.

Although knowledge about the spatial extent of flood events is obviously essential, little research has been devoted to studying the spatial dependence structure of hydrological events, both in general terms and at different spatial scales. Keef *et al.* (2009) for the first time proved the ability of a statistical method to map the joint occurrence of flood events in Great Britain. Schneeberger and Steinberger (2018) transferred the approach to the Austrian Province of Vorarlberg. Here, we applied the approach to Swiss catchments and extended the approach to consider different spatial scales of joint flood occurrences for high and extreme streamflows in Swiss catchments. The two spatial dependence measures introduced by Keef *et al.* (2009) are used to describe and map the spatial dependence of streamflow at four different scales. We tried to find catchments in which high streamflow and frequent floods were likely to occur simultaneously, and at the same time, we wanted to identify rivers that responded independently. To do so, we extended previous studies by a cluster analyses based on the two measures proposed. In this way, we are able to a) delineate the spatial extent of different floods by evaluating catchments with similar responses, and b) detect how representative a specific site is for a certain region.

Switzerland is a flood-prone country, especially in its mountainous regions. It has been affected by severe flood events in the past several decades (e.g. July 1987, May 1999, August 2005, July 2007 and October 2011) and, therefore, characterization

of the spatial dependence of floods is of interest for institutions involved in flood risk management. Furthermore, despite its relatively small area, Switzerland encompasses a variety of different landscape structures and hydro-meteorological regions, leading to diverse hydrological flow patterns (Weingartner and Aschwanden 1992). This results in different flood-generating mechanisms and causes flood events that only affect certain regions of the country. Nevertheless, the quantity and quality of runoff time series is sufficient for the study conducted. In fact, 56 runoff time series with record lengths of at least 50 years, spanning from low-lying catchments in the Swiss Plateau to high-alpine catchments, are available.

This paper is structured as follows. First, the study area and the spatial organization of the investigated rivers are presented. Then, we explain how the temporal and spatial dependences were estimated and which approach was used to cluster high streamflows. The presentation of the spatial dependence structure and the subsequent clustering is combined with a reflective discussion. Finally, we draw some conclusions and discuss possible implications of the results.

Study area and data

Switzerland covers an area of approximately 41 300 km^2 and has elevations ranging from 193 m above sea level (m a.s.l.) (Lake Maggiore) to 4634 m a.s.l. (Dufourspitze). A variety of landscapes with different hydrological processes are found at small spatial scales, e.g. the hilly Jura limestones in the northwest, the rather flat Swiss Plateau, and the Alpine areas with moist mountain reaches intersected by inner-alpine dry valleys (Figure 1). Major European rivers originate in the Swiss Alps, such as the Rhine, the Rhone, the Ticino (a tributary of the Po) and the Inn (a tributary of the Danube), which drain into the North Sea, the Mediterranean Sea, the Adriatic Sea and the Black Sea, respectively. Thus, from a hydrological perspective, Switzerland can be subdivided into

the four basins of the above-mentioned rivers.

[Figure 1 near here]

Before the dependence structure of streamflow can be analysed, categorizing the non-nested catchments into meso- and macro-scales was necessary. This enables the inspection of spatial dependence structures within and across scales. Otherwise, the results would be dominated by relatively high spatial dependence among river gauges located at just one river. As we aimed to analyse the spatial dependencies of high streamflow events at different scales, we needed to find as many river gauging stations with sufficient record lengths as possible; this enabled us the analysis at the desired scale. Out of the available Swiss gauging stations, we selected those with a record length of at least 50 years and deselected rivers heavily affected by human activity. The resulting 56 gauging stations were aligned to four different scales of interest (Figure 2): Scale Macro1 (M1) comprises the three main basins in Switzerland (Rhine, Rhone, Ticino). Though the Inn catchment would belong to M1 as well, no gauging station within Switzerland met the required criteria (length and naturalness). The tributaries of the Rhone and Rhine represent the Macro2 (M2) scale. The catchments comprising the Macro3 (M3) scale meet one of two criteria: (a) their catchment size is greater than 1000 km^2, or (b) they are smaller than 1000 km^2 but are important for regional coverage. The scales M1 to M3 comprise stations with record lengths of approximately 100 years. Finally, the most extensive set of catchments represent the meso-scale (<1000 km^2) headwater catchments, which are tributaries of the M3 catchments with record lengths of at least 50 years. The different scales are organized in a nested structure, in which the catchments within each level are arranged side-by-side (Figure 2).

[Figure 2 near here]

Methods

The study focuses on the analysis of high and extreme streamflow events, i.e. events that exceed a certain threshold. Throughout this article, we use the pth quantile of a set of observations X to define the threshold $q_p(X)$, meaning that observations above $q_p(X)$ have a probability p of not being exceeded. This quantile value, or non-exceedence probability, is referred to as the level of extremeness.

The definition of a flood event is an essential aspect when analysing the temporal dependence of streamflow at individual sites and the spatial patterns of streamflow peaks between several sites. A joint high-flow event is when the maximum flow at individual sites occurs simultaneously within a certain time interval with length L. The length L is determined by the approach described in the next paragraph and is applied in a preparatory step before spatial dependence analysis is conducted.

Temporal dependence of peaks

The dataset used in this study came from daily river gauge measurements, denoted by $D_{i,t}$, where i is an element of the investigated gauges and t is the observation time. To identify independent peaks, we analysed the runoff time series $D_{i,t}$ to determine the average time interval with a length L in which flood peaks at each site occur. Here, we asked for the level of extremeness of runoff on the days immediately before and after the flood peak to determine the probability that $q_p(X)$ was exceeded. Thus, following the idea of Schneeberger and Steinberger (2018) the probability of peaks with length L ($L \geq 1$) at site i can be expressed as

$$R_i(p, L) = \Pr\left(D_{i,(t,\dots,t+L-1)} \geq q_p \middle| D_{i,t} \geq q_p \wedge D_{i,t-1} < q_p \wedge D_{i,t+L} < q_p\right) \quad (1)$$

The number of sites is denoted by n. This measure shows that peaks with a certain length L (in days) and defined by the threshold $q_p(D)$ have a probability $R_i(p, L)$. The probability that peaks last for longer than one day reads as follows (e.g. for 2 days): $R_i(p, L \leq 2)$ and is calculated by summing up $R_i(p, L = 1)$ and $R_i(p, L = 2)$. The average probability of flood peaks is defined by

$$\mathrm{R}(p, L) = \frac{1}{n} \sum_{i=1}^{n} R_i(p, L) \quad (2)$$

For a certain level of extremeness, the average time interval with length L in which events usually occur can be deduced for individual sites by applying equation (1), and the average event length for a group of sites (e.g. sites of level M1) can be calculated with equation (2). The event length L is required for data preparation before the spatial dependence measures can be applied.

Spatial dependence measure

In addition to calculating temporal dependence of peaks at a certain site, we defined a widespread joint flood event as a hydrological condition in which multiple sites experience high streamflow. The spatial dependence analysis (i.e. the analysis of simultaneous occurrence of high streamflow among different sites) was done by calculating the conditional probability that a certain river i (dependent site) exceeded a certain level of extremeness, given that the runoff at a conditioning site (denoted by j) was above the same level of extremeness.

In order to consider lagged observation at different sites, we calculated block maxima for the spatial dependence analysis. Two different block maxima, Q_j and Q_i, defined by L, were determined for the conditioning site and the dependent site in a slightly different way. For the calculation of Q_j at conditioning site j, the highest

discharge was selected from regularly spaced blocks, as defined by the time interval of length L. Q_i was calculated as the highest value within a block defined by L, which was centred around the occurrence of values from conditioning site j. Figure 3 provides examples for the selection of block maxima of the conditioning site (left) and dependent sites (remaining three panels).

[Figure 3 near here]

The spatial dependence measure $P_{i,j}(p)$ can be considered an exploratory measure of bivariate dependence and is defined as (Keef *et al.* 2009):

$$P_{i,j}(p) = \Pr(Q_i > q_p(Q_i) | Q_j > q_p(Q_j)) \quad (3)$$

where $P_{i,j}(p)$ is the probability that the dependent site i exceeds the threshold $q_p(Q_i)$, given that site j is extreme as well. The thresholds $q_p(Q_j)$ and $q_p(Q_i)$ are based on two different block maxima Q_j (conditioning site) and Q_i (dependent site). A second spatial dependence measure $N_j(p)$ describes the average probability over all dependent sites i that are extreme (excluding site j), given that site j is also high (exceeding a threshold, $q_p(Q_i)$). $N_j(p)$ is defined as (Keef *et al.* 2009):

$$N_j(p) = \frac{\sum_{i \neq j} \Pr(Q_i > q_p(Q_i) | Q_j > q_p(Q_j))}{n-1} \quad (4)$$

where $N_j(p)$ can be interpreted as a summary measure that shows whether certain sites experience similar high streamflow occurrence.

Cluster analysis of high streamflow

Cluster analysis is a rather objective procedure in which a set of objects is divided into groups such that objects within a cluster are as similar as possible. For the cluster analysis, the investigated objects are the time series, which contain information on

whether the block maxima Q exceeds a certain threshold $q_p(Q)$. The threshold $q_p(Q)$ depends on the non-exceedence probability p. As block maxima, the highest discharge of regular spaced blocks are used (cf. Q_j in Figure 3). A binary time series C_i for each site i is generated, where $C_i = Q_i > q_p(Q_i)$. By combining binary time series from all stations, the cluster input variable $\boldsymbol{C}$ is generated, which is defined as $\boldsymbol{C} = [C_1, C_2, \dots, C_n]$. The input variable $\boldsymbol{C}$ for the cluster analysis is a binary matrix that contains information about whether a certain level of extremeness is exceeded at a certain time and site. The cluster analysis aims to identify groups/regions that react similarly in terms of high streamflow occurrence. This can be achieved by applying the k-means cluster method, which is a widely applied non-hierarchical clustering technique (Kaufman and Rousseeuw 1990). This algorithm partitions n observations into k clusters by minimizing the average squared distance of data to obtain the centroid of each cluster (Kaufman and Rousseeuw 1990). The steps are repeated until convergence has been reached. The consistency of the resulting clusters can be measured or evaluated by methods such as the silhouette value and the Calinski-Harabasz criterion (Calinski and Harabasz 1974, Kaufman and Rousseeuw 1990).

Results

Average duration of high-flow events

Time series of daily averages (D) from 56 river gauging stations with an average length of 91.7 years were used to determine the average duration of high-flow events (Table 1). The river gauging data in Switzerland are based on continuous measurements with *a posteriori* averaging to determine daily means. To delineate jointly occurring high streamflow events, the common definition of event length L for all streamflow quantiles was required. Based on the high flows exceeding the threshold $q_{p=0.997}(D)$, we show

the determined event length L at all sites in Figure 4. The temporal dependence measure $R_i(p, L)$ shows the percentage of peaks, defined by $q_p(D)$, with a certain time lag L at each site. For example, at the westernmost site depicted in Figure 4 (Rhone at Chancy, Rho@Cha), 73.5% of all high streamflows were equal to or exceeded the $q_{p=0.997}(D)$ threshold and lasted for 1 day (blue fraction). Accordingly, fractions of 17.2%, 3.5%, 3.5%, and 2.3%, were found for events that equalled or exceeded the threshold for 2 (cyan), 3 (yellow), 4 (red), and 5 or more days, respectively. An especially homogeneous pattern from all sites can be seen in Figure 4. Applying equation (2), we found that approximately 70% of all events peaked for only one day, though 18% of events exceeded the threshold for a maximum of two days. Longer event lengths were rare for most sites. Exceptions to this pattern can be found in the Inn catchment (easternmost river), in one river in the Ticino (southern rim), and in some sites in the north-central and northwest regions. A closer look at these sites revealed locations next to lakes (east and north-central) and a location in a karstic environment (northwest site); these cause specific conditions that alter the average length of flood peaks. In total, 94% of peaks, defined by $p = 0.997$, were found to have a length of 1, 2 or 3 days ($R(p = 0.997, L \leq 3) = 0.94$). A similar finding can be found for other levels of extremeness, such as $p = 0.99$ and $p = 0.9992$, as shown in Figure 5. In addition, we tested for a general dependence of the event length on the catchment size, but, interestingly, found no relationship. Based on these analyses of daily mean data D_i, a shared value for event length L across all levels of extremeness seems legitimate and was set to three days in forthcoming analyses of this study.

[Table 1 near here]

[Figure 4 and 5 near here]

Spatial dependence of river flow

Having determined the event length ($L = 3$ days), we can shift to the main focus of this study, i.e. the spatial dependencies of high and extreme streamflows in Switzerland and possible spatial patterns. For this purpose, the maximum values in time intervals with length L (i.e. block maxima Q) are used for further analyses. The terms "high" and "extreme" streamflows are understood as runoff above certain thresholds $q_p(Q)$. The quantile values that define thresholds for "high" streamflow are between $p = 0.95$ and $p = 0.99$ and for "extreme" streamflow they are between $p = 0.995$ and $p = 0.999$. As the event length was determined to be 3 days, a threshold of $q_{p=0.99}(Q)$ roughly refers to one 3-day event per year; a threshold of $q_{p=0.999}(Q)$ refers to a 10-year event. Please note that in this study we focus on frequent floods (return period of up to 10 years) rather than very extreme events with higher return periods.

Looking at the spatial dependence measure $N_j(p)$ for high streamflows in the three main Swiss basins (scale M1), a clear asymptotic independence is visible (Figure 6). This means that the more extreme the streamflow is at one site, the more unlikely it is that this level of extremeness will simultaneously occur in one of the other major rivers. In fact, we found it was very unlikely that a flood event affected the basins with the same level of high intensity across the entirety of Switzerland. In addition, this finding clearly suggests there are different hydro-meteorological regions with largely independent high and extreme streamflow occurrences that are caused by different meteorological precursors.

[Figure 6 near here]

A more detailed dependence analysis focused solely on the Rhine basin and was represented by the M1 river gauge Rhine at Basel (Rheinhalle) Rhi@BRh, which covers approximately 36 000 km^2. We selected the Rhine basin for this detailed analysis

because several potentially flood-prone Swiss cities and metropolitan areas, such as Zurich, Basel and Berne, are located in this area, and it includes large tributaries, e.g. the Aare, the Reuss and the Limmat. Furthermore, the Rhine basin comprises three M2, eight M3, and 29 meso-scale catchments and has a relatively high number of river gauges, allowing for cross-scale dependence analysis.

The Rhine River at Basel mainly comprises two large tributaries, the Aare and the High Rhine, which is located upstream from the confluence with the Aare. We found higher spatial dependence of high and extreme streamflow occurrences at the Rhine at Basel (Rhi@BRh) and the Rhine at Rekingen (Rhi@Rek) than at the Rhine and the Aare at Untersiggenthal (Aar@Unt) (Figure 7(b)). The spatial dependence measure $P_{i,j}(p)$ between Rhi@BRh and Birse at Münchenstein (Bir@Mün) was even lower. For extreme streamflows, the dependence measure $P_{i,j}(p)$ decreases for all bivariate combinations at scale M2, meaning they become less dependent.

The higher spatial dependences between Rhi@BRh and Rhi@Rek compared to the Upper Rhine and Aar@Unt was surprising, as the Aare is the larger river and generates more discharge (Figure 7(a)). In terms of spatial dependence, the characteristics of frequent floods in the Rhine at Basel, the Aare, and the High Rhine upstream from the confluence with the Aare can be explained as follows: for a 10-year flood at the Rhine in Basel (Rhi@BRh, i.e. ~3700 $m^3 s^{-1}$), a 10-year flood of only one of the two main tributaries is not sufficient, because a 10-year flood at Aar@Unt is ~2000 $m^3 s^{-1}$ and at Rhi@Rek is ~1500 $m^3 s^{-1}$)[1]. The Aare flood wave is typically characterized by a defined flood peak, while the flood curve at Rhi@Rek is much more dampened due

[1] The official return values corresponding to 10-years flood events are taken from the website of the Federal Office of the Environment in Switzerland (https://www.hydrodaten.admin.ch/en/)

to the retention effect of Lake Constance. Hence, the basic shape of the flood curve in Basel is determined by the Aar@Unt that is additionally scaled by the flood wave of Rhi@Rek. Although the discharge volume of both tributaries is sufficient to cause a threshold exceedence at Rhi@BRh, flood peaks undershot the threshold due to the dampened effect of Lake Constance. Only if the flood wave at Rhi@Rek is pronounced or superposed by the inflow of Thu@And and Tös@Nef (and therefore exceeding a certain threshold), the flood waves of Rhi@Rek and Aar@Unt can cumulate to result in a distinct flood curve in Rhi@BRh. Thus, the probability of the latter is more dependent on the flood wave of Rhi@Rek than Aar@Unt.

If we look at the responses of M3 gauges, when the streamflow is high at Rhi@BRh (Figure 7(c)), the spatial dependence is mostly lower than the correlation with the Aare and High Rhine at Rekingen M2 sites. The highest correlation for moderate to high streamflow could be found between the Rhine (Rhi@BRh) and both the Limmat at Zurich (Lim@Zür) and the Reuss at Mellingen (Reu@Mel). Interestingly, the share from Thur at Andelfingen (Thu@And) and Töss at Neftenbach (Tös@Nef) are more important for extreme streamflows, implying that the rivers Thur and Töss have frequently severely contributed to extreme streamflow in Basel. This can be explained by the absence of an upstream lake providing attenuating effects, and the amplifying effects of their discharges adding to the already-high discharge from the Aare catchment. In contrast, high streamflows in several other M3 Rhine tributaries are attenuated by downstream lakes (cf. Figure 7(a)). Thus, large M3 catchments, such as the Alpine Rhine at Diepoldsau (Rhi@Die, the largest M3 catchment), which is situated upstream of Lake Constance, and the Aare at Bern (Aar@Ber, the third largest M3 catchment), which is situated upstream of Lake Biel, are weakly correlated with Rhi@BRh. This is also true for smaller tributaries, such as the Orbe (Orb@Orb), which

is located upstream of Lake Neuchatel and Lake Biel. Apparently, upstream lakes considerably reduce the spatial dependence of M3 sites.

[Figure 7 near here]

The time series of macro-scale sites used so far, have a length of roughly 100 years. Further analysis focuses on the meso-scale, which encompasses data with a length of 50 years.

Cluster of high streamflow

Analysing the spatial dependence of high streamflow provides information on the joint occurrence of peaks at different spatial scales. The interpretation of the dependence was found to be straightforward at coarse scales but became more difficult at finer scales. The results of the spatial dependence analysis at meso-scales was not visually interpretable because of the large number of meso-scale sites (hence, the meso-scale is not shown here). Thus, the spatial pattern of high streamflow in meso-scale catchments was investigated with a cluster analysis. A k-means cluster algorithm was used to identify groups that react similarly in terms of high streamflow occurrence (Figure 8(a)). The cluster analysis was performed for different levels of extremeness (p), ranging from 0.9 to 0.99 in increments of 0.01. The identified clusters were found to be independent from p values. This is shown in Figure 8(b), where each colour represents one class, assuring the consistent denotation of clusters. Approximately half of the sites were distinctly associated with one individual cluster for the investigated levels of extremeness. For the remaining sites, a predominant cluster (allocation of ≥75%) was found. These results indicate that the displayed clusters of high streamflow occurrence are robust for meso-scale catchments, irrespective of the investigated level of extremeness.

[Figure 8 near here]

In addition to the selection of p, the effect of the number of cluster classes was analysed. By applying a cluster analysis with only two classes, the Swiss meso-scale sites were subdivided into northern (including northern pre-alpine regions) and southern sites (including the Alps and Ticino). For a higher number of cluster classes, further groups were identified, such as the North, the Alpine foreland, and the Ticino. In terms of allocation to clusters based on different levels of extremeness and cluster validation criteria (i.e. silhouette values and Calinski-Harabasz criterion), the best results were discovered by applying five cluster classes. The following five regions had similar patterns regarding the joint occurrence of high streamflow events: (i) "North-West" (including the Jura limestone mountains), (ii) the "North-East", (iii) the northern "Alpine foreland", (iv) the "central Aps", and (v) the "Ticino" (Figure 9(a)).

The spatial dependence measure $N_j(p)$ was applied to the members of each cluster to test the dependence structure within each group. The sites with the highest $N_j(p)$ in each cluster (averaged over the range of investigated p) were selected as representative sites for their respective cluster (marked with an additional circle in Figure 8(a)). The cluster representatives for "North-West", "North-East", "Alpine foreland", "central Alps", and "Ticino" were found to be the Suze (Suz@Son), the Thur (Thu@Jon), the Muota (Muo@Ing), the Reuss (Reu@And), and the Cassarate (Cas@Pre), respectively. The independence of these clusters can be seen in Figure 9, which plots the spatial dependence measure $P_{i,j}(p)$ of each cluster representative to the other cluster representatives (Figure 9(b–f)). An asymptotic independence can be found for Suze, Reuss, and Cassarate, and only slight spatial dependencies were found for Thur and Muota. Thus, asymptotic independence is not restricted to the major rivers in Switzerland (M1 scale) but holds widely true for the identified cluster representatives

derived from meso-scale catchments. This means that high streamflows in the main Swiss basins, as well as in the identified cluster regions, (i.e. their representatives) did not occur simultaneously in the past.

[Figure 9 near here]

Discussion

This study was conducted to determine if and to what extent joint flood occurrences exist, and it also assessed possible spatial patterns of high and extreme streamflow events in Switzerland. When analysing the three major rivers of Switzerland at the macro-scale, the asymptotic independence suggests there are independent factors triggering the largest floods. Similarly, distinct patterns emerged from the clusters identified in the meso-scale catchments within each major river network; again, this indicates that the three major rivers are asymptotically independent.

This is good news, as the probability of frequent flood events affecting all major rivers at once is minimal. Northern and southern catchments are very unlikely to experience a flood at the same time. These findings are in line with results of Froidevaux and Martius (2016), who identified different regions in Switzerland that are affected by prevailing storm tracks, and, more specifically, by the integrated vapour transport near the mountains. The five clusters found here also indicate it is unlikely multiple regions will be jointly affected by a flood event. Hence, these findings contain valuable information concerning the potentially affected populations, infrastructure and buildings, and economic loss.

However, how robust are these identified independent structures, and what are the possible reasons for them? We compared the identified cluster regions with the hydro-meteorological maps or analyses for Switzerland. A comparison with the nine hydro-climatic regions of Switzerland (see citation and map in Schmocker-Fackel and

Naef 2010) visually revealed only coarse relationships: A northeast and a southern region are similar to the regions found in this study, but the northwest, central, and eastern hydro-climate regions cannot be traced in our delineation. In addition, the three flood regions (northwest, northeast, and southern) derived from annual maximum series (AMS) correlations by Schmocker-Fackel and Naef (2010) and also the closely related storm-track-affected regions delineated by Froidevaux and Martius (2016) showed only moderate similarities at a higher aggregation level: E.g. the southern region consists of southern and mountainous region, the northeast, and the northwest (that strongly overlap) comprise all other meso-scale catchment clusters. Indeed, our meso-scale spatial pattern seems more closely linked to the main discharge regimes (Aschwanden and Weingartner 1985). These runoff characteristics divide Switzerland into the Jura mountain region in the northwest, the Swiss Plateau, the pre-Alps, the Alps, and the southern flank of Ticino, thus agree quite well with our flood regions (Figure 7(b)). In contrast to previously mentioned studies, the runoff regimes are an expression of climatological features and catchment characteristics, such as elevation and geology. In this respect, the regime types are only proxies for the underlying flood defining processes. Additional detailed in-depth analyses might find a direct link between spatial flood patterns and catchment characteristics. Although, the runoff regimes nicely aligned with our meso-scale pattern of joint flood occurrences, they do not fully explain the identified separation of northeastern and northwestern flood regions especially within the Swiss plateau. This division can be explained by the storm-track related regions of Froidevaux and Martius (2016) that result in the extreme floods clusters of Schmocker-Fackel and Naef (2010). In this respect, the identified frequent-flood regions are a clear expression of hydro-meteorological conditions that combine flood-triggering meteorological processes (e.g. storm tracks) with catchment characteristics

(e.g. topography, geology). This finding is in line with the conclusion Keef *et al.* (2009) drew from the study on Great Britain floods, highlighting the influence of catchment characteristics on spatial flood patterns, and the superior role of mountainous areas on precipitation patterns (thus flood triggering meteorological processes). This gives reasons for a more universal and convincing explanation for the causes of frequent-flood regions.

One of the surprising findings in our study was the independency of catchment size and event length. Keef *et al.* (2009) highlighted the different behaviour of slowly responding permeable catchments and fast-responding impermeable catchments, respectively. We assume that this catchment characteristic may camouflage the expected positive correlation between catchment size and event length. But this remains an open question for future analyses.

Differences between the flood regions discovered in the present study and the study by Schmocker-Fackel and Naef (2010) might also be influenced by the different flood levels considered and the fact that our approach ensures that the streamflow thresholds are exceeded during the same event. Hence, we conclude that the presented regional joint flood occurrence maps clearly add information to existing studies.

As the study focuses on spatial patterns of frequent floods, a time series with a high temporal resolution (hourly data) would be preferred. Such data would reflect the hydrological responses of small catchments more precisely than mean daily data. Nevertheless, we used mean daily data as input data because they are available for a much longer period. The Swiss time series with an hourly resolution typically date back to 1974. The minimum length of our investigated time series with a daily resolution is 50 years for meso-scale gauges and approximately 100 years for macro-scale gauges. Thus, higher-resolution time series are insufficient in terms of observation length.

Nevertheless, we tested the spatial patterns of frequent floods based on hourly data for a shorter time period and found quite similar results. This gives us confidence that the influence of the data resolution on observed spatial patterns is less important, and our choice to perform the analysis using the longest time periods available has no obvious drawbacks.

Conclusion

In this article, we present an evaluation of the spatial dependence and delineated regions of high streamflow events in Switzerland for different levels of extremeness and at different scales. Although our results are supported by existing studies on runoff regimes and existing studies on flood regions, we clearly add new and valuable information to these studies. From an application point of view, our results show that the major rivers were affected by frequent floods at different times. Furthermore, flood defence planners, insurance companies, and other stakeholders can use the results to estimate regions where floods are likely to occur together or independently. However, the present work focuses on frequent floods, whereas temporal and spatial dependence analyses were conducted using empirical data. In studies related to flood risk, high return periods (i.e. 1-in-100 years or less frequently) determined by applying flood frequency analyses are of interest. This level of extremeness cannot be captured using the applied methods, because the occurrence date of investigated peaks is required for spatial dependence analysis.

From a scientific point of view, the applied method presented in Keef *et al.* (2009), which was extended in terms of data preparation in this study, proved to supply plausible, yet new, results for Switzerland. Furthermore, the application of a cluster analysis based on the dependence structures gained from the statistical approach revealed a strong added value as distinct flood regions could be delineated.

Thus, future applications in other countries or even continent-wide are promising, although data availability and quality might not always meet the Swiss standard. Furthermore, the approach is flexible enough to extend the analyses to joint flood occurrences of different flood levels (i.e. extreme streamflow in river A might be strongly correlated with high streamflow in river B) or even to delineate regions of joint drought occurrences. All of these applications are beyond the scope of this study but might be subject to future work.

Acknowledgements

We would like to thank Thomas Steinberger for the valuable comments on cluster analysis. We acknowledge the Federal Office of the Environment in Switzerland for their generous provision of discharge data. We would like to thank Nina Bosshard, two anonymous reviewers, and the editors for providing valuable comments and handling the manuscript.

References

Aschwanden, H., and Weingartner, R., 1985. *The runoff regimes in Switzerland (Die Abflussregimes der Schweiz)*. Bern: Geogr. Inst. Univ. Bern.

Barredo, J.I., 2009. Normalised flood losses in Europe: 1970-2006. *Natural Hazards and Earth System Sciences,* 9, 97–104.

Becker, A., and Grünewald, U., 2003. Disaster management. Flood risk in Central Europe. *Science (New York, N.Y.),* 300 (5622), 1099.

Bezzola, G.R., and Hegg C., 2007. *Ereignisanalyse Hochwasser 2005,. Teil 1 - Prozesse, Schäden und erste Einordnung*. Bern: Eidgenössische Forschungsanstalt WSL.

Blöschl, G., *et al.,* 2013. The June 2013 flood in the Upper Danube Basin, and comparisons with the 2002, 1954 and 1899 floods. *Hydrology and Earth System Sciences,* 17 (12), 5197–5212.

Calinski, T., and Harabasz, J., 1974. A dendrite method for cluster analysis. *Communications in Statistics - Theory and Methods,* 3 (1), 1–27.

Castellarin, A., and Pistocchi, A., 2012. An analysis of change in alpine annual maximum discharges: implications for the selection of design discharges. *Hydrological Processes,* 26 (10), 1517–1526.

Excimap, 2007. *Handbook on good practices for flood mapping in Europe*.

Falter, D., *et al.,* 2015. Spatially coherent flood risk assessment based on long-term continuous simulation with a coupled model chain. *Journal of Hydrology,* 524, 182–193.

Falter, D., *et al.,* 2016. Continuous, large-scale simulation model for flood risk assessments: Proof-of-concept. *Journal of Flood Risk Management,* 9 (1), 3–21.

Froidevaux, P., and Martius, O., 2016. Exceptional integrated vapour transport toward orography. An important precursor to severe floods in Switzerland. *Quarterly Journal of the Royal Meteorological Society,* 142 (698), 1997–2012.

Hall, J., *et al.,* 2014. Understanding flood regime changes in Europe: a state-of-the-art assessment. *Hydrology and Earth System Sciences,* 18 (7), 2735–2772.

Hilker, N., Badoux, A., and Hegg, C., 2009. The Swiss flood and landslide damage database 1972–2007. *Natural Hazards and Earth System Sciences,* 9 (3), 913–925.

Kaufman, L., and Rousseeuw, P.J., eds., 1990. *Finding Groups in Data*. Hoboken, NJ, USA: John Wiley & Sons, Inc.

Keef, C., Svensson, C., and Tawn, J.A., 2009. Spatial dependence in extreme river flows and precipitation for Great Britain. *Journal of Hydrology,* 378 (3–4), 240–252.

Köplin, N.*, et al.,* 2014. Seasonality and magnitude of floods in Switzerland under future climate change. *Hydrological Processes,* 28 (4), 2567–2578.

Kundzewicz, Z.W., 2015. Climate change track in river floods in Europe. *Proceedings of the International Association of Hydrological Sciences,* 369, 189–194.

Madsen, H.*, et al.,* 2014. Review of trend analysis and climate change projections of extreme precipitation and floods in Europe. *Journal of Hydrology,* 519, 3634–3650.

Merz, B., Nguyen, V.D., and Vorogushyn, S., 2016. Temporal clustering of floods in Germany. Do flood-rich and flood-poor periods exist? *Journal of Hydrology,* 541, 824–838.

Moel, H. de*, et al.,* 2015. Flood risk assessments at different spatial scales. *Mitigation and Adaptation Strategies for Global Change,* 20 (6), 865–890.

Schmocker-Fackel, P., and Naef, F., 2010. More frequent flooding? Changes in flood frequency in Switzerland since 1850. *Journal of Hydrology,* 381 (1-2), 1–8.

Schneeberger, K.*, et al.,* 2017. A Probabilistic Framework for Risk Analysis of Widespread Flood Events. A Proof-of-Concept Study. *Risk analysis: an official publication of the Society for Risk Analysis*.

Schneeberger, K., and Steinberger, T., 2018. Generation of Spatially Heterogeneous Flood Events in an Alpine Region—Adaptation and Application of a Multivariate Modelling Procedure. *Hydrology,* 5 (5).

Schröter, K.*, et al.,* 2015. What made the June 2013 flood in Germany an exceptional event? A hydro-meteorological evaluation. *Hydrology and Earth System Sciences,* 19 (1), 309–327.

Thieken, A.H.*, et al.,* 2016. The flood of June 2013 in Germany. How much do we know about its impacts? *Natural Hazards and Earth System Sciences,* 16 (6), 1519–1540.

Weingartner, R., and Aschwanden, H., 1992. Discharge Regime - the Basis for the Estimation of Average Flows. *In:* Federal Office for the Environment FOEN, ed. *Hydrological Atlas of Switzerland.* Bern, CH.

Figure captions

Figure 1. The major river networks in Switzerland (Rhine, Inn, Ticino, and Rhone: see legend) and the locations of the 56 gauging stations used in this study. Please refer to the Table 1 for full names.

Figure 2. Time series from river gauges (see Table 1 for abbreviations): those in boxes are used for the analysis; descriptions in parentheses are not used.

Figure 3. Data preparation and understanding of joint events.

Figure 4. Map of Switzerland showing the probability $R_i(p, L)$ that high streamflow events defined by $p = 0.997$ last a certain time L and display a very homogenous pattern with a dominant event length of only 1 day.

Figure 5. (a) Length of occurrence of high streamflow $R_i(p, L)$ with four segments representing the results for $L = 1$, 2, 3, and 4 days, respectively. (b) Summary of the probabilities for different event length by cumulating the median probabilities for each event threshold.

Figure 6. Spatial dependence $N_j(p)$ against non-exceedence probability p of streamflow in M1 catchments.

Figure 7. (a) Schematic drawing of river reaches (M1–M3) in the Rhine basin. The line thickness corresponds to the mean values of the appropriate AMS. (b–c) Spatial dependence measures $P_{i,j}(p)$ against non-exceedence probabilities p (conditioning site (j): Rhi@BRh) for (b) dependent sites: M2 sub-catchments of Rhine; and (c) dependent sites: M3 sub-catchments of Rhine.

Figure 8. Cluster analysis of high-flow events for meso-scale catchments: (a) predominant cluster over different p values (p = 0.9–0.99); cluster representatives are additionally marked with circles, and (b) cluster assignment for the 10 different p values, illustrated by colour codes, and their fraction displayed in the pie charts.

Figure 9. (a) Map of Switzerland and (b–e) spatial dependence measures $P_{i,j}(p)$ of cluster representatives for (b) Suze at Sonceboz (Suz@Son) – North-West, (c) Thur at Jonschwil (Thu@Jon) – North-East, (d) Muota at Ingenbohl (Muo@Ing) – Alpine

foreland, (e) Reuss at Andermatt (Reu@And) – central Alps, and (f) Cassarate at Pregassona (Cas@Pre) – Ticino.

Table 1. Selected river gauging stations. Abbreviated names of gauging stations consist of the first three letters of rivers and sites, respectively.

Abbrev.	Level	ID	River	Name	Data available since	Area (km^2)	Elevation of gauge (m a.s.l.)	Ave. elevation (m a.s.l.)	Mean of AMS ($m^3 s^{-1}$)
Rhi@BRh	M1	2289	Rhein	Basel, Rheinhalle	1869	35 897	246	1025	2887
Rho@Cha	M1	2174	Rhone	Chancy, Aux Ripes	1904	10 323	336	1580	973
Tic@Bel	M1	2020	Ticino	Bellizona	1911	1515	220	1680	890
Rhi@Rek	M2	2143	Rhein	Rekingen	1904	14 718	323	1080	1175
Aar@Unt	M2	2205	Aare	Untersiggenthal, Stilli	1904	17 601	326	1050	1551
Bir@Mün	M2	2106	Birs	Münchenstein, Hofmatt	1916	911	268	740	154
Arv@Gen	M2	2170	Arve	Geneve, Bout du Monde	1904	1976	380	1370	494
ARh@Die	M3	2473	Rhein	Diepoldsau, Rietbrücke	1919	6119	410	1800	1336
Thu@And	M3	2044	Thur	Andelfingen	1904	1696	356	770	593
Tös@Nef	M3	2132	Töss	Neftenbach	1921	342	389	650	122
Lim@Zür	M3	2099	Limmat	Zürich, Unterhard	1906	2176	400	1190	342
Reu@Mel	M3	2018	Reuss	Mellingen	1904	3382	345	1240	493
Emm@Wil	M3	0155	Emme	Wiler, Limpachmündung	1921	939	458	860	283
Aar@Ber	M3	2135	Aare	Bern, Schönau	1917	2945	502	1610	361
Orb@Orb	M3	2378	Orbe	Orbe, Le Chalet	1906	333	445	1130	93
VoR@Ila	Meso	2033	Vorderrhein	Ilanz	1910	776	693	2020	383
Lan@Fel	Meso	2150	Landquart	Felsenbach	1921	616	571	1800	189
Wer@SaB	Meso	2187	Werdenberger Binnenkanal	Salez	1930	180	432	1020	67
Sit@App	Meso	2112	Sitter	Appenzell	1912	74.2	769	1252	76
Mur@Wän	Meso	2126	Murg	Wängi	1954	78.9	466	650	30
Thu@Jon	Meso	2303	Thur	Jonschwil, Mühlau	1966	493	534	1030	349
RhB@StM	Meso	2139	Rheintaler Binnenkanal	St. Margrethen	1919	360	399	880	78
Aac@Sal	Meso	2312	Aach	Salmsach, Hungerbühl	1961	48.5	406	480	20
Sih@Zür	Meso	2176	Sihl	Zürich, Sihlhölzli	1925	336	412	1060	144
Lin@Mol	Meso	2372	Linth	Mollis, Linthbrücke	1914	600	436	1730	197
Gla@Her	Meso	2305	Glatt	Herisau, Zellersmühle	1961	16.2	679	840	30
Muo@Ing	Meso	2084	Muota	Ingenbohl	1917	316	438	1360	173
Reu@And	Meso	2087	Reuss	Andermatt	1910	192	1427	2280	117
Sar@Sar	Meso	2102	Sarner Aa	Sarnen	1907	267	469	1280	32
Lor@Fra	Meso	2125	Lorze	Frauenthal	1913	259	390	690	19

Alp@Ers	Meso	2299	Alpbach	Erstfeld, Bodenberg	1960	20.6	1022	2200	22
Eng@Buo	Meso	2481	Engelberger Aa	Buochs, Flugplatz	1916	227	443	1620	79
Kle@Emm	Meso	2634	Kleine Emme	Emmen	1936	478	430	1051	298
Lan@Hut	Meso	2343	Langeten	Huttwil, Häberenbad	1966	59.9	597	766	20
Aar@Bri	Meso	2019	Aare	Brienzwiler	1905	554	570	2150	206
Lüt@Gst	Meso	2109	Lütschine	Gsteig	1908	379	585	2050	124
Sim@Obe	Meso	2151	Simme	Oberwil	1921	344	777	1640	83
Gür@Bel	Meso	2159	Gürbe	Belp, Mülimatt	1922	117	522	837	33
Sen@Thö	Meso	2179	Sense	Thörishaus, Sensematt	1928	352	553	1068	161
Sar@Bro	Meso	2160	Sarine	Broc, Chateau d'en bas	1922	639	682	1520	220
Bro@Pay	Meso	2034	Payerne, Caserne d'aviation	Broye	1920	392	441	710	149
Are@Bou	Meso	2480	Areuse	Boudry	1904	377	444	1060	100
Erg@Lie	Meso	2202	Ergolz	Liestal	1934	261	305	590	61
Dra@LeC	Meso	2117	Drance de Bagnes	Le Chable, Villette	1911	254	810	2630	47
Vis@Vis	Meso	2351	Vispa	Visp	1922	778	659	2660	152
Rho@Bri	Meso	2346	Rhone	Brig	1965	913	667	2370	269
Sal@Bri	Meso	2342	Saltina	Brig	1966	77.7	677	2050	29
Gra@Aig	Meso	2203	Grande Eau	Aigle	1935	132	414	1560	38
Dou@Oco	Meso	2210	Doubs	Ocourt	1921	1230	417	950	226
Suz@Son	Meso	2307	Suze	Sonceboz	1961	150	642	1050	30
Bre@Lod	Meso	2086	Brenno	Loderio	1930	397	348	1820	190
Cas@Pre	Meso	2321	Cassarate	Pregassona	1962	73.9	291	990	47
Tre@Pon	Meso	2167	Tresa	Ponte Treas, Rocchetta	1901	615	268	800	103
Ber@Pon	Meso	2262	Berninabach	Pontresina	1954	107	1804	2617	50
Cha@LaP	Meso	2263	Chamuerabach	La Punt-Chamues-ch	1954	73.3	1720	2549	18
Inn@StM	Meso	2105	Inn	St. Moritzbad	1907	155	1770	2400	31

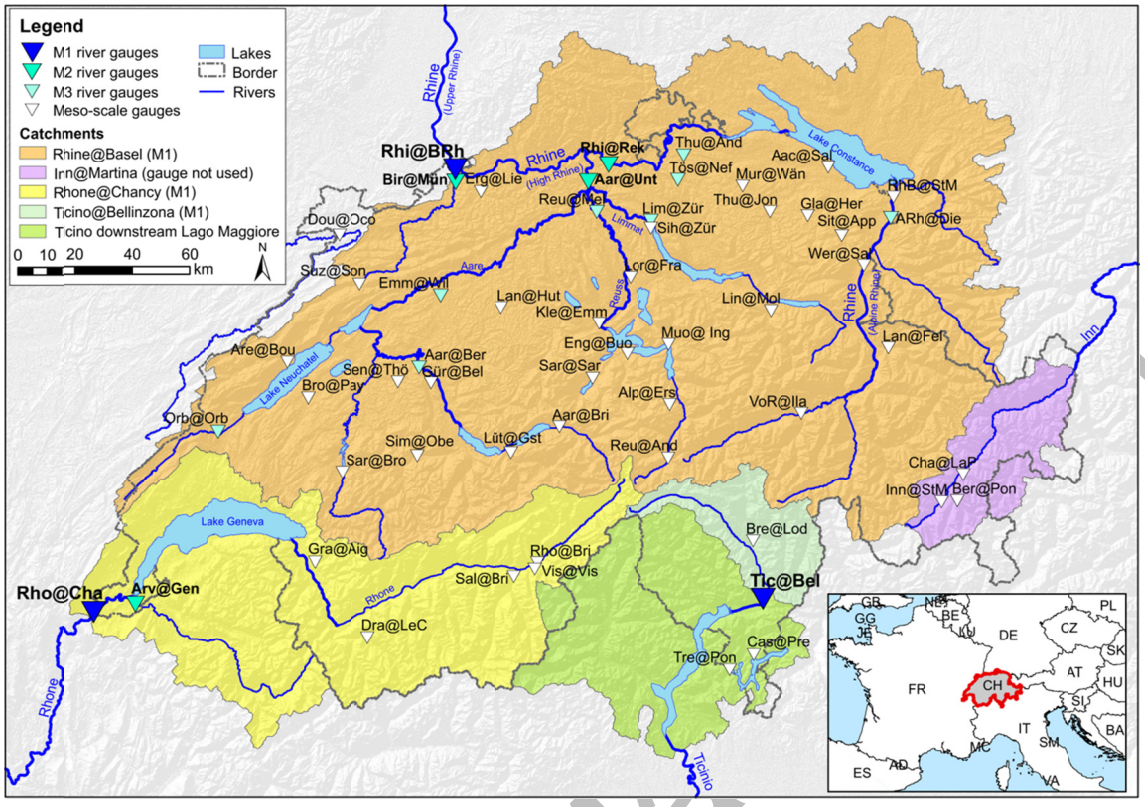

Figure 1

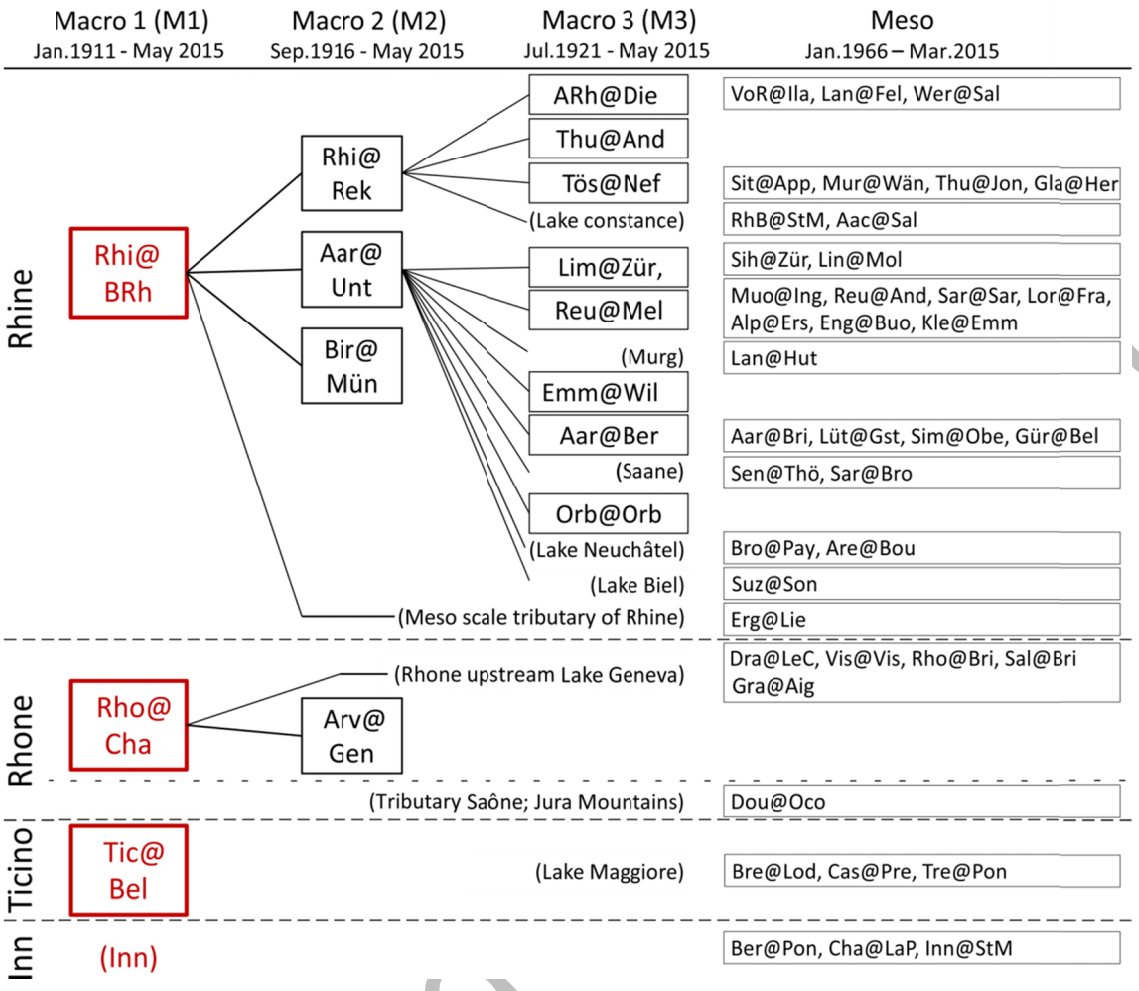

Figure 2

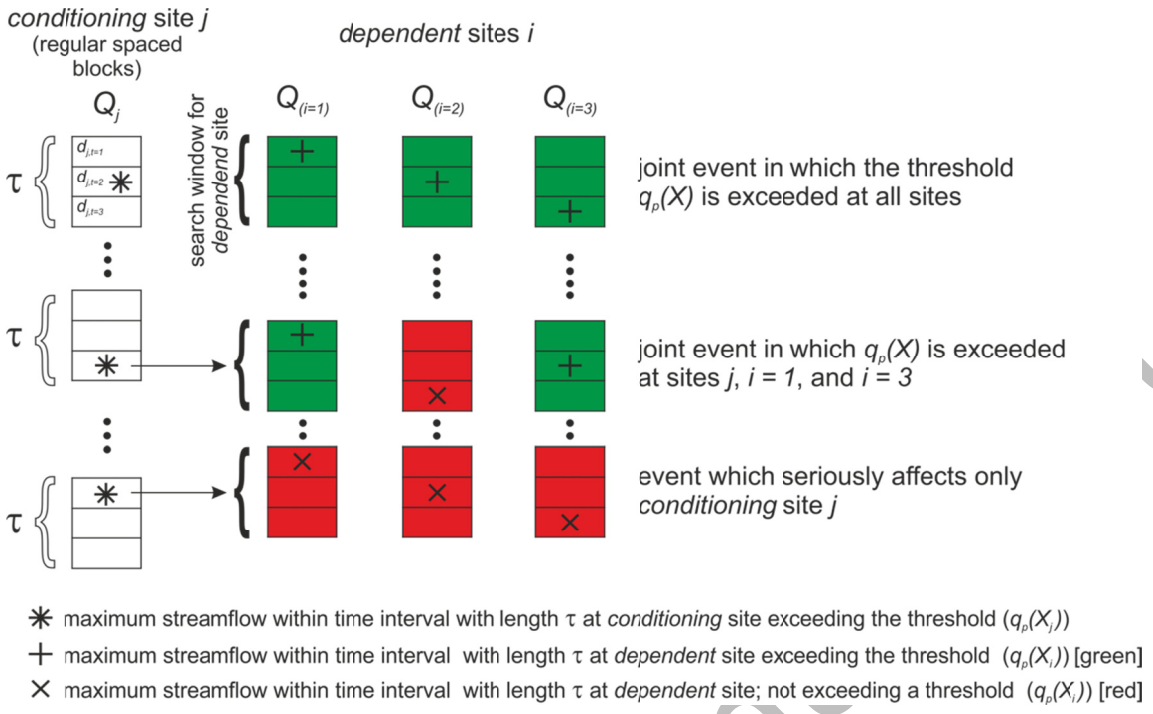

Figure 3

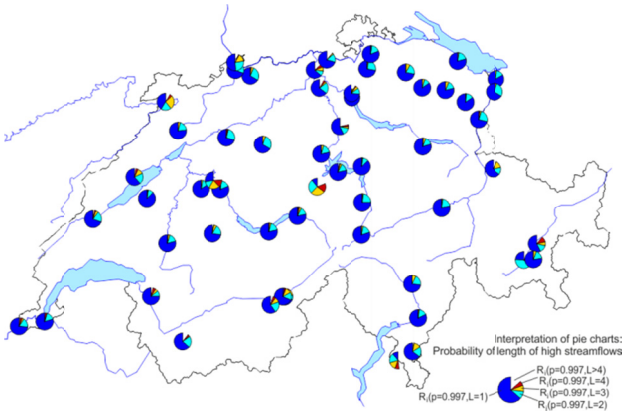

Figure 4

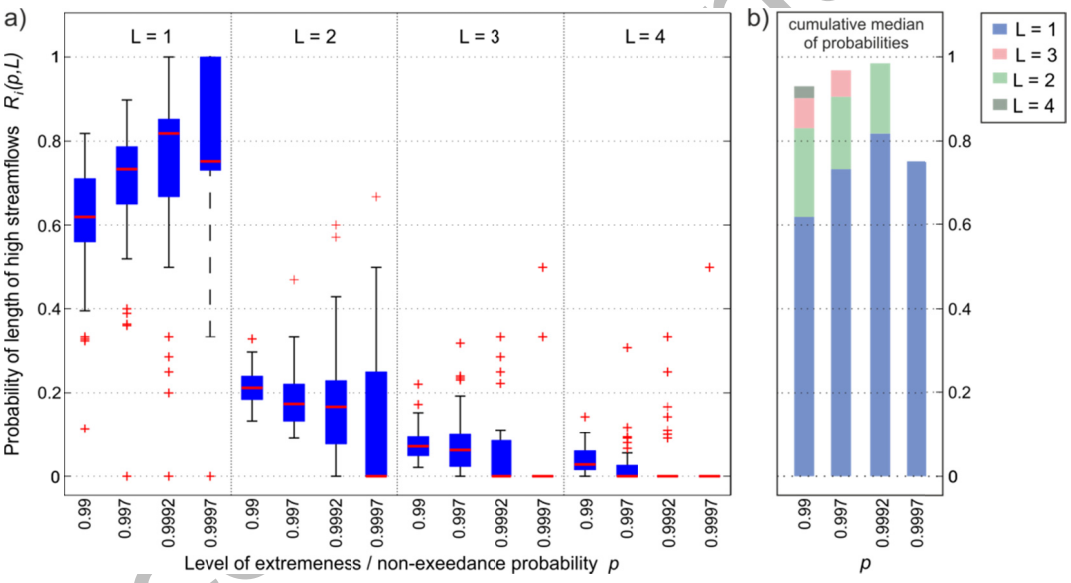

Figure 5

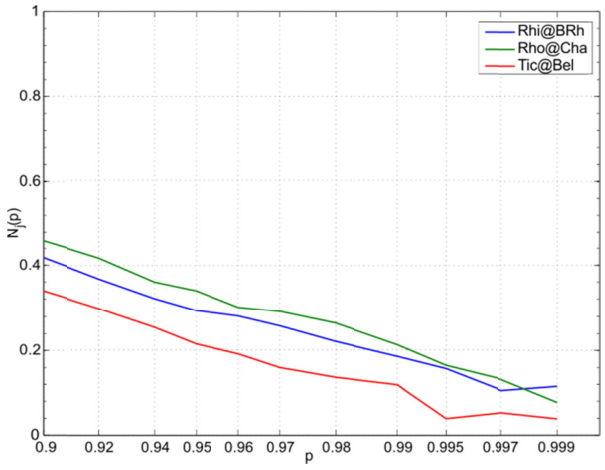

Figure 6

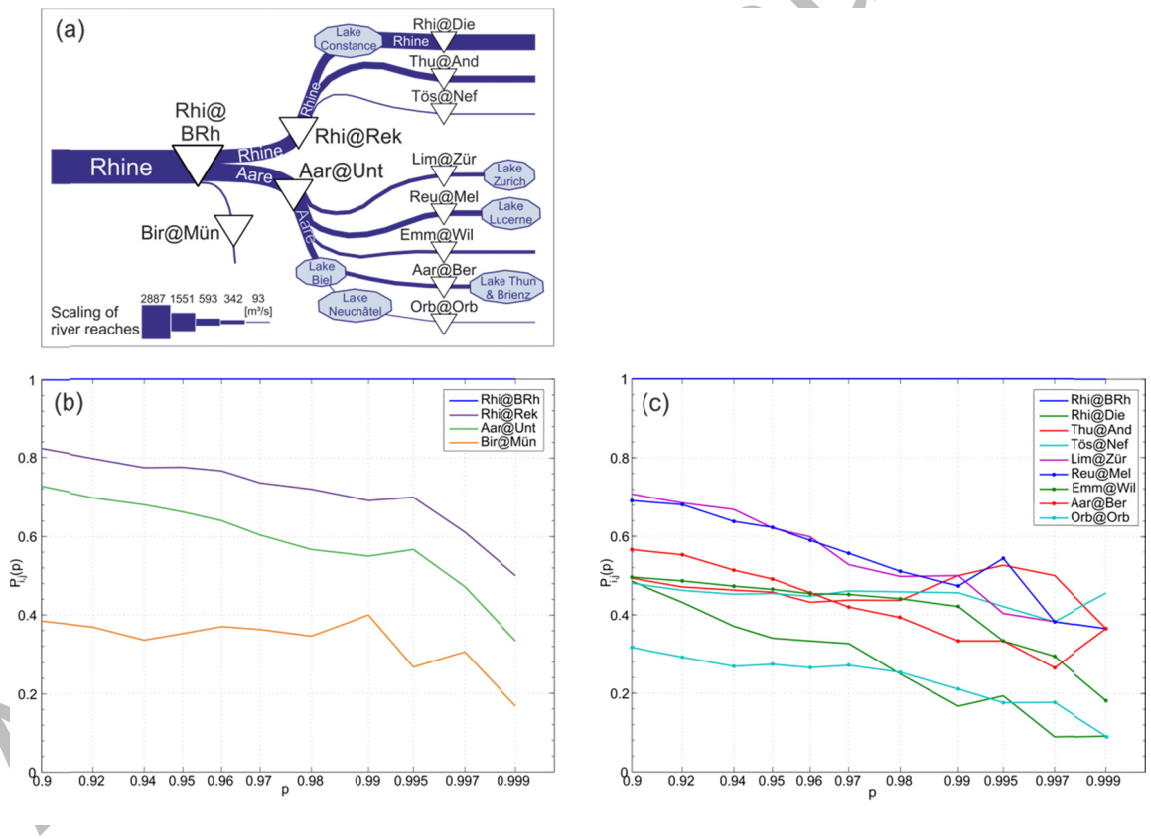

Figure 7

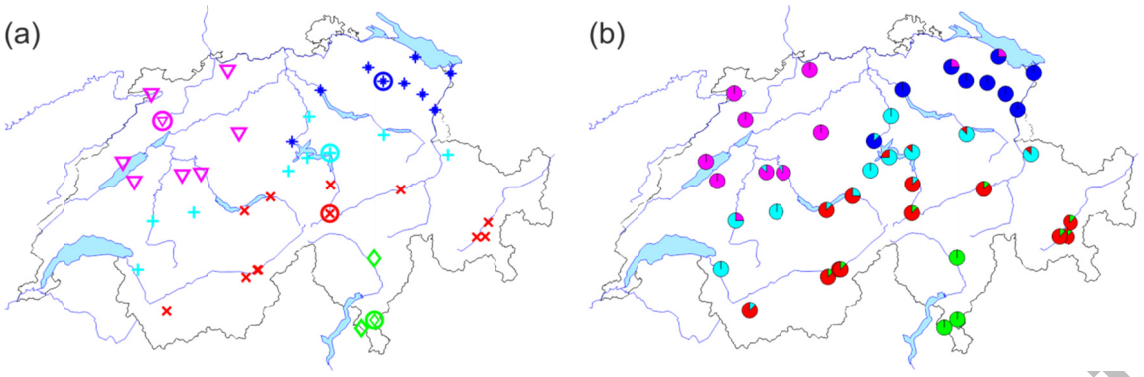

Figure 8

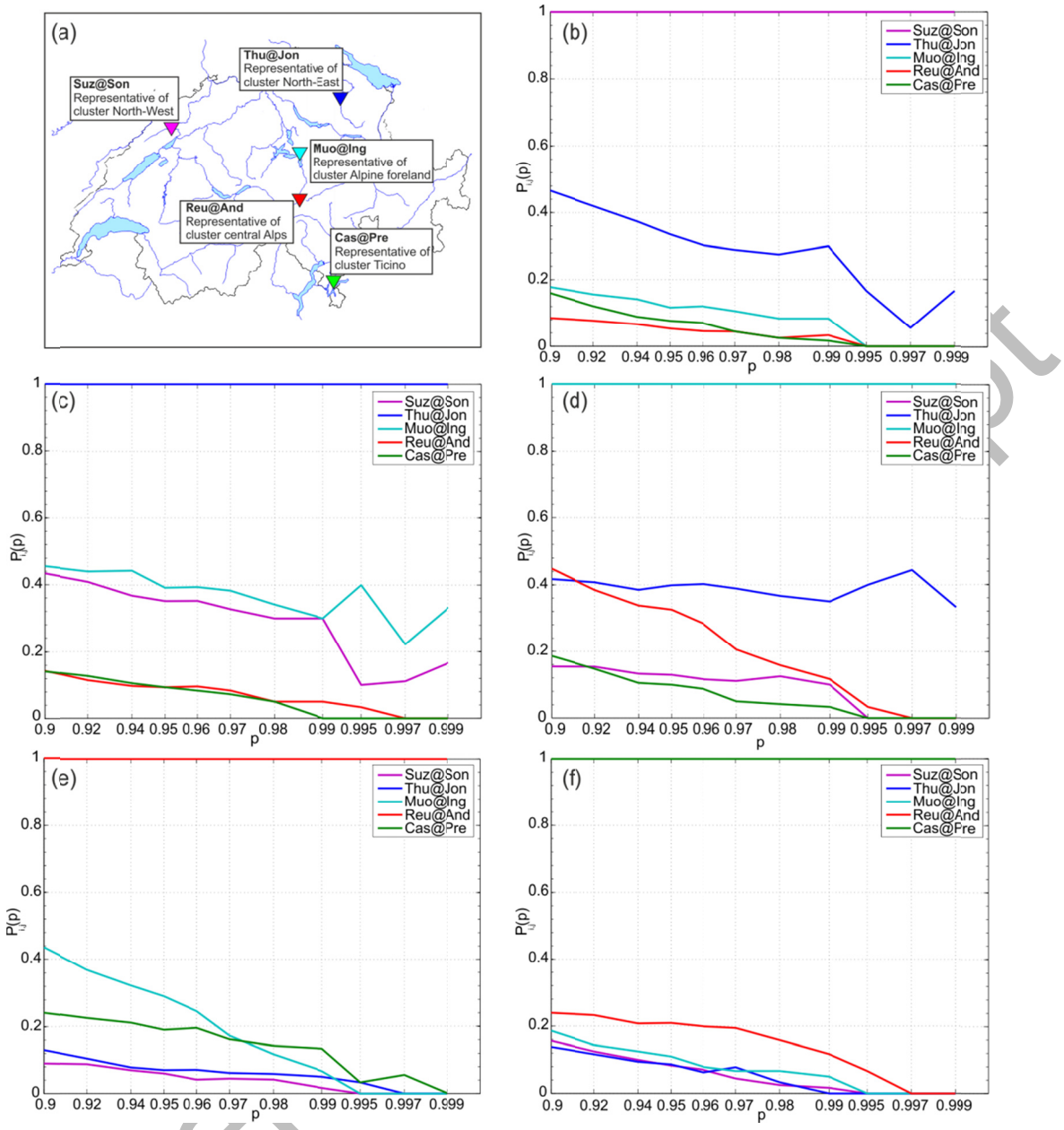

Figure 9